Letter

High-frequency phonons drive large phonon-drag thermopower in semiconductors at high carrier density

Chunhua Li,[1] Nakib H. Protik,[2] Navaneetha K. Ravichandran,[3] and David Broido[1,*]

[1]*Department of Physics, Boston College, Chestnut Hill, Massachusetts 02467, USA*

[2]*Institut für Physik and IRIS Adlershof, Humboldt-Universität zu Berlin, 12489 Berlin, Germany*

[3]*Department of Mechanical Engineering, Indian Institute of Science, Bangalore 560012, India*

(Received 17 November 2022; revised 17 January 2023; accepted 26 January 2023; published 7 February 2023)

It has been well established that (i) the thermopower of semiconductors can be enhanced through a phenomenon known as the drag effect, and (ii) the drag enhancement involves only low-frequency acoustic phonons and benefits from low electron densities and low temperatures. Using first-principles calculations we show that large drag enhancements to the thermopower are possible at *high carrier density* even at room temperature and arise from *high-frequency* acoustic phonons. A fascinating example is cubic boron arsenide (BAs) for which the calculated room temperature drag enhancement of the thermopower exceeds an order of magnitude at a high hole density of 10^{21} cm^{-3}. This remarkable behavior stems from the simultaneously weak phonon-phonon and phonon-hole scattering of the high-frequency phonons in BAs that become drag active at high carrier densities through electron-phonon interactions. This work advances our understanding of coupled electron-phonon nanoscale transport and introduces an unexpected paradigm for achieving large thermopowers.

DOI: 10.1103/PhysRevB.107.L081202

Introduction. The Seebeck thermopower, S, is a fundamental transport parameter that gives a measure of the magnitude of the electric current generated in response to an applied temperature gradient. A related quantity, the Peltier thermopower, Q, gives a measure of the magnitude of the heat current generated by an applied electric field. These thermopowers are often studied theoretically under the Bloch assumption [1–3] in which phonons are artificially constrained to remain in thermal equilibrium. The Bloch assumption yields the so-called diffusion thermopowers. In reality, the phonon and electron subsystems are coupled through the electron-phonon interactions. Then, the momentum exchange between these two subsystems increases the Seebeck and Peltier thermopower magnitudes above the diffusive contributions—a phenomenon known as electron-phonon drag.

The drag contribution to the thermopower of semiconductors is largest at low charge-carrier density where it is controlled by phonon-phonon scattering [3,4]. At higher carrier densities, collision rates between phonons and carriers increase further, dissipating the phonon current and thereby reducing the drag thermopower. This is known as the saturation effect [4]. The saturation effect has been confirmed by measurement and by *ab initio* calculations [5–9].

In the typical range of carrier densities studied in semiconductors, electron-phonon interactions couple electrons and holes mainly to low-frequency acoustic phonons [3,4,7]. Moreover, low-frequency phonons have smaller phonon-phonon collision rates than do their high-frequency counterparts. These features cause the low-frequency phonons to dominate the contributions to the drag thermopower for not too high carrier densities.

In this work, using first-principles calculations, we show that in certain materials, a window of higher carrier densities exists where the drag contributions to the thermopower come primarily from *high-frequency acoustic phonons*. We find that these contributions dominate over their low-frequency counterparts and are also much larger than the corresponding diffusive contributions. A striking example is cubic boron arsenide (BAs), which is found to have exceedingly large drag enhancements of the thermopower at high hole densities, more than an order of magnitude larger than the corresponding diffusive contributions. This behavior arises from the combination of weak phonon-phonon and phonon-carrier scattering for the high-frequency phonons in BAs. Even silicon (Si) shows unexpectedly large drag enhancements at high carrier densities from drag-active high-frequency phonons. These extraordinary results reveal a previously unidentified picture of thermoelectric transport, in which the drag contribution to the thermopower can dominate not only in the region of low carrier densities, but also in the regime of high carrier densities.

Coupled electron-phonon transport in the Peltier picture. We present the theory of the thermopower in the Peltier picture [3,4] in which an applied electric field, $\mathbf{E}$, in a doped semiconductor generates a charge current density, $\mathbf{J}_e = \sigma\mathbf{E}$, as well as electronic and phonon contributions to the heat current density, $\mathbf{J}_Q^{el} = TQ_c\mathbf{J}_e$ and $\mathbf{J}_Q^{ph} = TQ_{ph}\mathbf{J}_e$, the latter being the drag contribution created by momentum transfer to the phonon subsystem from the charge current through the electron-phonon scattering. Here, σ is the electrical conductivity while Q_c and Q_{ph} are the carrier and phonon contributions to the total Peltier thermopower, $Q = Q_c + Q_{ph}$. We have taken the crystal structure of the material to be cubic, for which the transport coefficients are scalars.

*Corresponding author: broido@bc.edu

Application of a small electric field, **E**, in a doped semiconductor creates a nonequilibrium charge-carrier distribution function, which can be linearized as $f_\nu = f_\nu^0 + f_\nu^1$ where f_ν^0 is the equilibrium Fermi distribution and $f_\nu^1 = -f_\nu^0(1-f_\nu^0)\mathbf{J}_\nu \cdot \mathbf{E}/(k_B T)$. Through electron-phonon coupling, a nonequilibrium phonon distribution function is created: $n_\lambda = n_\lambda^0 + n_\lambda^1$ where n_λ^0 is the Bose distribution and $n_\lambda^1 = -n_\lambda^0(n_\lambda^0+1)\mathbf{G}_\lambda \cdot \mathbf{E}/(k_B T)$. Here, k_B is the Boltzmann constant, T is the temperature, ν designates the electron state with electron band index, n, and wave vector, $\mathbf{k}$, λ represents a phonon mode with phonon branch index, j, and wave vector, $\mathbf{q}$, while $\mathbf{J}_\nu$ and $\mathbf{G}_\lambda$ are the carrier and phonon deviation functions in response to the electric field. The relevant transport coefficients, σ, Q_c, and Q_{ph}, can be expressed as [8–11]

$$\sigma = \frac{2e}{3Vk_BT}\sum_\nu f_\nu^0\left(1-f_\nu^0\right)\mathbf{v}_\nu \cdot \mathbf{J}_\nu, \tag{1}$$

$$Q_c = -\frac{2}{3\sigma Vk_BT^2}\sum_\nu f_\nu^0\left(1-f_\nu^0\right)(\varepsilon_\nu - \mu)\mathbf{v}_\nu \cdot \mathbf{J}_\nu, \tag{2}$$

$$Q_{ph} = -\frac{1}{3\sigma Vk_BT^2}\sum_\lambda n_\lambda^0\left(n_\lambda^0+1\right)\hbar\omega_\lambda \mathbf{v}_\lambda \cdot \mathbf{G}_\lambda. \tag{3}$$

In the equations, e is the magnitude of the electron charge, V is the crystal volume, ε_ν and $\hbar\omega_\lambda$ are the carrier and phonon energies, $\mathbf{v}_\nu$ and $\mathbf{v}_\lambda$ are the corresponding group velocities, and μ is the chemical potential.

The Kelvin-Onsager relation [3,12] mandates the equivalence of the Seebeck and Peltier thermopowers: $S = Q = Q_c + Q_{ph}$. Under the Bloch assumption ($Q_{ph} = 0$), the Kelvin-Onsager relation becomes $Q_c = S_{\text{diff}}$, where S_{diff} is the diffusive contribution to the Seebeck thermopower. The corresponding drag contribution is $S_{\text{drag}} = S - S_{\text{diff}}$, which is in most cases almost the same as Q_{ph}.

Large drag thermopower driven by high-frequency phonons. We investigated the drag thermopower in two materials, Si and BAs, using a first-principles approach, in which the coupled electron and phonon Boltzmann transport equations in the presence of both an applied electric field and a temperature gradient were solved using the ELPHBOLT code [11]. Since BAs samples have been found to be p type [13], we consider hole doping for both BAs and Si. Along with σ, Q_c and Q_{ph}, S and the electronic and phonon contributions to the thermal conductivity, k_e and k_{ph}, were also determined. The computational details are provided in the Supplemental Material [14].

We focus first on the intrinsic behavior in which charge carriers scatter only from phonons through the electron-phonon interactions, and phonons scatter from carriers, from other phonons through anharmonic three-phonon interactions, and from the mass fluctuations produced by random isotopic disorder. The effect on the BAs thermopower from four-phonon scattering, which is known to significantly suppress the k_{ph} of BAs, will be considered below. Figure 1(a) shows the calculated Seebeck coefficients for BAs (solid red curve) and Si (solid blue curve) as a function of hole density, p, at 300 K. The calculated results for Si show good agreement with the measured data (black circles, from Ref. [6]) across a wide range of densities up to around $10^{19}\,\text{cm}^{-3}$, supporting the predictive capability of the approach. Similarly good

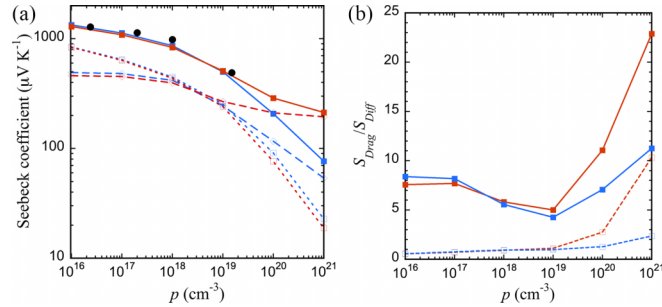

FIG. 1. Seebeck coefficients for BAs and Si as a function of hole density, p, at 300 K. (a) BAs: solid red curve; Si: solid blue curve. Black circles are measured data for Si [6]. Short-dashed and long-dashed curves give S_{diff} and S_{drag}. (b) Ratio of S_{drag} to S_{diff} for BAs (red) and Si (blue) at 300 K (dashed) and at 100 K (solid).

agreement with experiment has been obtained in prior *ab initio* calculations [7,11,26]. The short-dashed and long-dashed curves give S_{diff} and S_{drag}, respectively. S_{diff} is largest at low density and decreases monotonically with increasing density. This characteristic behavior connects the two limits of lightly doped semiconductors, where the entropy transported per charge is large, consistent with the nondegenerate Fermi statistics, and metals where degenerate statistics apply and the entropy per charge is small.

At low densities, S_{drag} approaches a constant value. With increasing density ($10^{17} - 10^{19}\,\text{cm}^{-3}$), S_{drag} decreases, consistent with the saturation effect described above, and at a similar rate to that of S_{diff} for both Si and BAs. Above $10^{19}\,\text{cm}^{-3}$, a striking change in behavior occurs, with S_{drag} decreasing more slowly than S_{diff}. As a result, S_{drag} becomes much larger than S_{diff} at high density for both Si and BAs. Furthermore, while the S for BAs and Si are similar around and below $10^{19}\,\text{cm}^{-3}$, above $10^{19}\,\text{cm}^{-3}$, S for BAs decreases more slowly than that for Si resulting in much larger S for BAs. For example, at $T = 300$ K and $p = 10^{21}\,\text{cm}^{-3}$, the S calculated for BAs is $213\,\mu\text{V K}^{-1}$, almost three times higher than the corresponding value for Si of $76\,\mu\text{V K}^{-1}$. These features are highlighted in Fig. 1(b), which shows the ratio of S_{drag} to S_{diff} for BAs and Si as a function of p, at 300 K and at 100 K. Around and below $10^{19}\,\text{cm}^{-3}$ the $S_{\text{drag}}/S_{\text{diff}}$ ratios are similar for BAs and Si at both temperatures. Above $10^{19}\,\text{cm}^{-3}$, the $S_{\text{drag}}/S_{\text{diff}}$ ratios increase for both materials, but with noticeably sharper increases in BAs.

To understand this surprising behavior, it is useful to use the Peltier picture and to examine the spectral contribution to the drag thermopower, $Q_{ph}(\nu)$, which is defined through

$$Q_{ph} = \int_0^{\nu_{max}} Q_{ph}(\nu)d\nu, \tag{4}$$

where ν_{max} is the maximum phonon frequency. Physically, $Q_{ph}(\nu)d\nu$ gives the contribution to Q_{ph} in the frequency range between ν and $\nu + d\nu$. $Q_{ph}(\nu)$ is obtained by equating the right-hand sides of Eqs. (3) and (4) as

$$Q_{ph}(\nu) = -\frac{1}{3\sigma Vk_BT^2}\sum_\lambda n_\lambda^0\left(n_\lambda^0+1\right)\hbar\omega_\lambda \mathbf{v}_\lambda \cdot \mathbf{G}_\lambda \delta(\nu - \nu_\lambda), \tag{5}$$

where $\delta(\nu)$ is the delta function.

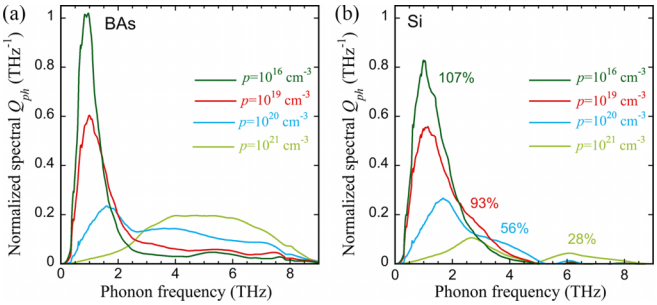

FIG. 2. Normalized spectral phonon contributions to the room temperature Q_{ph}. (a) BAs; (b) Si; for four hole densities: $p = 10^{16}\,\mathrm{cm}^{-3}$, $10^{19}\,\mathrm{cm}^{-3}$, $10^{20}\,\mathrm{cm}^{-3}$, and $10^{21}\,\mathrm{cm}^{-3}$. The percentages in (b) indicate the scaling factor, Q_{ph} (Si)/Q_{ph} (BAs), weighting the Si contributions relative to those in BAs.

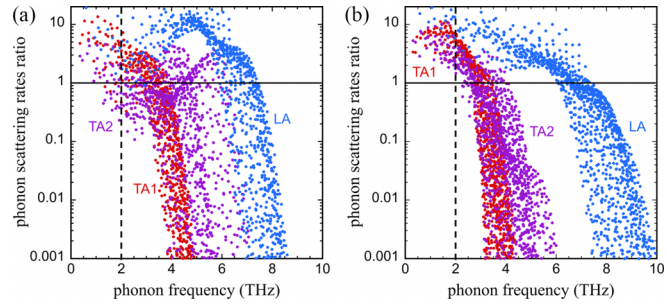

FIG. 3. (a) Ratio of phonon-hole scattering rates to three-phonon scattering rates in BAs for hole density, $p = 10^{21}\,\mathrm{cm}^{-3}$ and at 300 K; (b) same for Si. Ratios are broken down by acoustic phonon branches. Red: transverse acoustic 1 (TA1); purple: transverse acoustic 2 (TA2); blue: longitudinal acoustic (LA). Vertical dashed black lines separate regions of low- and high-frequency phonons.

Figure 2 shows $Q_{ph}(\nu)$ at room temperature for BAs [Fig. 2(a)] and Si [Fig. 2(b)] for four hole densities: $p = 10^{16}\,\mathrm{cm}^{-3}$, $10^{19}\,\mathrm{cm}^{-3}$, $10^{20}\,\mathrm{cm}^{-3}$, and $10^{21}\,\mathrm{cm}^{-3}$. For each curve in Fig. 2, we numerically evaluated Eq. (5) for $Q_{ph}(\nu)$ and normalized by the corresponding total Q_{ph} of BAs at that hole density. In the low-density range, $10^{15} - 10^{18}\,\mathrm{cm}^{-3}$, the spectral Q_{ph} are almost identical to each other so only the plot for $p = 10^{16}\,\mathrm{cm}^{-3}$ is shown. Above $10^{19}\,\mathrm{cm}^{-3}$, there is a clear shift of spectral weight from low-frequency phonons to high-frequency phonons for both BAs and Si. The reduced contributions from low-frequency phonons are expected from the saturation effect. The dominant contributions from high-frequency phonons are not.

A second striking feature is that BAs acquires much more spectral weight from high-frequency phonons than does Si. This is highlighted in Fig. 2(b), where the Si spectral Q_{ph} at each density is normalized by the corresponding Q_{ph} for BAs. For example, at 300 K and $p = 10^{21}\,\mathrm{cm}^{-3}$, the Q_{ph} of Si is only 28% that of BAs at the same density [27].

To clarify why high-frequency phonons contribute to Q_{ph} at high density, we first note that at low carrier density, in which nondegenerate statistics apply, conservation of momentum and energy in carrier-phonon scattering processes admits only phonons with energies [28] $\hbar\omega \lesssim 2v\sqrt{3mk_BT}$, assuming a parabolic band and Debye phonon dispersion. Here, m is the carrier effective mass and v is the Debye velocity of an acoustic phonon. The result is independent of p. For $m = 1$ and $v = 6500$ m/s (reasonable choices for both BAs and Si), $\omega/2\pi \lesssim 2$ THz at room temperature. In fact, for $p < 10^{19}\,\mathrm{cm}^{-3}$ about 80% (90%) of phonons contributing to the Q_{ph} for BAs and Si have frequencies below 2 THz at 300 K (100 K) (see Fig. S1 of the Supplemental Material [14]).

At high density, where degenerate statistics apply, the corresponding result is $\hbar\omega \lesssim 2\hbar v(3\pi^2 p)^{1/3}$ which increases with p and gives a frequency of around 6.5 THz for $p = 10^{21}\,\mathrm{cm}^{-3}$, consistent with the frequency range we find for acoustic phonon-hole scattering at that density. That high-frequency phonons can contribute to Q_{ph} while low-frequency phonons do not can be understood by comparing the phonon-hole scattering rates to the three-phonon scattering rates at high p shown in Fig. 3. For low-frequency phonons ($\lesssim$2 THz), the former significantly exceeds the latter thereby suppressing contributions to Q_{ph}. This is the normal saturation effect. In contrast, for many high-frequency phonons, phonon-hole scattering rates lie well below three-phonon scattering rates. Thus, the saturation effect on these phonons is weak allowing them to contribute more to Q_{ph}.

In BAs, the high-frequency acoustic phonons have unusually weak three-phonon scattering rates (see Fig. S2)—a feature that contributes to its ultrahigh k_{ph} [29–33]. Thus, high-frequency acoustic phonons have simultaneously weak phonon-hole and three-phonon scattering even at high hole densities, which allows them to provide much larger contributions to the drag thermopower of BAs compared to that of Si. Similarly, k_{ph} is negligibly suppressed by phonon-carrier scattering up to high carrier density (Fig. S3). Figure S3 shows that the same conclusion holds when including four-phonon scattering. In contrast, the k_{ph} of Si is sharply reduced, decreasing by around 50% at $p = 10^{21}\,\mathrm{cm}^{-3}$, as has been shown previously [34]. This striking difference occurs because undoped Si receives a larger fraction of spectral contributions to its k_{ph} from lower-frequency phonons for which phonon-hole scattering is much stronger than three-phonon scattering at $p = 10^{21}\,\mathrm{cm}^{-3}$. We emphasize that although the phonon-phonon scattering is stronger in Si than in BAs for high-frequency phonons, it is still weak compared with that of most other materials, which is critical in Si achieving the relatively large S_{drag} values in the high-density regime.

We note that while the contributions from high-frequency acoustic phonons to S_{drag} are large in BAs, the corresponding contributions from optic phonons are negligible. This follows in part from the small optic phonon populations resulting from the high optic phonon frequencies (∼20 THz). This same feature is critical to BAs having weak polar-optic phonon scattering rates for the charge carriers [35]. Other factors are the rapid dissipation of out-of-equilibrium optic phonons caused by their large phonon-phonon, phonon-isotope, and phonon-hole decay rates, and the small group velocities of the optic phonons.

Effects on BAs drag thermopower from four-phonon scattering. In undoped BAs at room temperature, the three-phonon scattering is so weak for some high-frequency acoustic phonons that it becomes comparable to the higher-order four-phonon scattering. The latter has been found to suppress k_{ph} by almost 50% [30–33]. To assess the effect of four-phonon

scattering on the thermopower of BAs, we have calculated the four-phonon scattering rates using the method described in Ref. [36] (see Supplemental Material [14] for detailed expressions) and incorporated them in the coupled electron-phonon transport calculations. We find a much weaker suppression of the BAs thermopower from four-phonon scattering. Below $p = 10^{19}\,\mathrm{cm}^{-3}$, the effect of four-phonon scattering on Q_{ph} and S is negligible because for the low-frequency phonons contributing to Q_{ph} in this density region, the four-phonon scattering rates are much smaller than the three-phonon scattering rates. At high densities, reductions in Q_{ph} are notably smaller (e.g., Q_{ph} and S are reduced by only 27% and 24%, respectively, for $p = 10^{21}\,\mathrm{cm}^{-3}$ at 300 K) than the corresponding reductions in k_{ph} because more of the spectral contributions to Q_{ph} occur at lower frequencies where four-phonon scattering is weak. Thus, the finding of large contributions to the BAs drag thermopower from high-frequency acoustic phonons still holds when including four-phonon scattering. As T is lowered below 300 K, four-phonon scattering weakens more rapidly than does three-phonon scattering, so the effect of four-phonon scattering on the BAs thermopower becomes negligible.

Effect of carrier and phonon scattering from impurities on drag thermopower. The calculations to this point have described the intrinsic transport properties in the absence of any extrinsic impurities. Thus, they give the optimum thermoelectric transport properties and drag contributions to the thermopower. Impurity atoms scatter both charge carriers and phonons thereby reducing the respective charge and heat currents. To assess the impact of such impurities on the drag thermopower of BAs and Si, carrier-impurity and phonon-impurity scattering were included in the transport calculations. Expressions for these scattering rates are given in the Supplemental Material [14]. Charge-impurity scattering produced only small changes to the thermopowers even at high densities, consistent with prior calculations performed at lower densities [7,8]. In Si, the phonon-impurity scattering causes surprisingly little change in S. In BAs, it has a much larger effect, reducing the room temperature Q_{ph} (S) by 86% (71%) at $p = 10^{21}\,\mathrm{cm}^{-3}$ (see Fig. S4). These larger reductions occur because BAs has larger spectral contributions to the intrinsic Q_{ph} from high-frequency phonons than does Si, and the phonon-impurity scattering rates are largest at high frequency. We note that Hall and thermopower measurements on Si and BAs have been performed up to hole densities exceeding $10^{20}\,\mathrm{cm}^{-3}$ [33,37–42]. However, we expect that the samples used have far more impurities and defects than considered in our thermopower calculations, preventing proper comparisons between theory and experiment.

Connection to drag thermopower in metals. In metals, phonons across the full phonon frequency spectrum are drag active [28]. However, in stark contrast to BAs and Si, the measured thermopower values for many metals are small, around $1\,\mu\mathrm{V\,K}^{-1}$, across a wide range of temperatures around and below 300 K [43]. It is interesting to examine the underlying physical reasons for this difference. Recent *ab initio* calculations [44,45] found much stronger three-phonon scattering rates in a large number of metals than those occurring in BAs and Si. This suggests that the small metallic thermopowers are caused by strong phonon-phonon scattering that rapidly dissipates the phonon current preventing efficient momentum exchange with the electron subsystem.

Conclusions. From *ab initio* calculations, we have demonstrated that large drag enhancements to the thermopower that arise from high-frequency acoustic phonons are possible. The onset of degenerate statistics for charge carriers that occurs for higher densities activates high-frequency acoustic phonons in the electron-phonon drag process. Then, the combination of weak phonon-phonon and phonon-carrier scattering for these high-frequency phonons, such as is found to occur in BAs, lead to exceptionally large thermopower enhancements exceeding by more than an order of magnitude the corresponding diffusive contributions. This behavior is in striking contrast to that found in the regime of low carrier densities where only low-frequency phonons are involved. These results give a novel paradigm for achieving large drag-enhanced thermopowers in materials. Moreover, they identify another remarkable property of BAs along with its high thermal conductivity and simultaneously high electron and hole mobilities [46,47].

These findings motivate a search for other materials with similarly large thermopower enhancements. Recently, computational studies have predicted that large diffusion thermopowers can occur in semimetals with asymmetric electronic density of states around the Fermi level [48]. Since the carrier density range in semimetals is comparable to the densities considered in this work, the present findings suggest that it may be possible to achieve both large drag and diffusion thermopowers in semimetallic systems.

This work was supported by the U.S. Department of Energy (DOE), Office of Science, Basic Energy Sciences (BES) under Award No. DE-SC0021071. D.B. and C.L. acknowledge the Boston College Linux clusters for computational resources and support. N.H.P. was supported by a Humboldt Research Fellowship from the Alexander von Humboldt Foundation, Bonn, Germany. We gratefully acknowledge Gang Chen of MIT along with Zhiwei Ding and Te-Huan Liu for providing us with their prior unpublished calculated results of the BAs phonon thermal conductivity as a function of hole density, which were similar to our results.

[1] F. Bloch, Zum elektrischen Widerstandsgesetz bei tiefen Temperaturen, Z. Phys. **59**, 208 (1930).

[2] R. Peierls, Zur theorie der elektrischen und thermischen leitfähigkeit von metallen, Ann. Phys. **396**, 121 (1930).

[3] J. M. Ziman, *Electrons and Phonons: The Theory of Transport Phenomena in Solids* (Oxford University Press, New York, 2001).

[4] C. Herring, Theory of the thermoelectric power of semiconductors, Phys. Rev. **96**, 1163 (1954).

[5] T. H. Geballe and G. W. Hull, Seebeck effect in Germanium, Phys. Rev. **94**, 1134 (1954).

[6] T. H. Geballe and G. W. Hull, Seebeck effect in silicon, Phys. Rev. **98**, 940 (1955).

[7] J. Zhou, B. Liao, B. Qiu, S. Huberman, K. Esfarjani, M. S. Dresselhaus, and G. Chen, *Ab initio* optimization of phonon drag effect for lower-temperature thermoelectric energy conversion, Proc. Natl. Acad. Sci. USA **112**, 14777 (2015).

[8] N. H. Protik and B. Kozinsky, Electron-phonon drag enhancement of transport properties from a fully coupled *ab initio* Boltzmann formalism, Phys. Rev. B **102**, 245202 (2020).

[9] C. Li, N. H. Protik, P. Ordejón, and D. Broido, Colossal phonon drag enhanced thermopower in lightly doped diamond, Mater. Today Phys. **27**, 100740 (2022).

[10] N. H. Protik and D. A. Broido, Coupled transport of phonons and carriers in semiconductors: A case study of *n*-doped GaAs, Phys. Rev. B **101**, 075202 (2020).

[11] N. H. Protik, C. Li, M. Pruneda, D. Broido, and P. Ordejón, The elphbolt *ab initio* solver for the coupled electron-phonon Boltzmann transport equations, npj Comput. Mater. **8**, 28 (2022).

[12] E. Sondheimer, The Kelvin relations of thermo-electricity, Proc. R. Soc. London, Ser. A **234**, 391 (1956).

[13] B. Lv, Y. Lan, X. Wang, Q. Zhang, Y. Hu, A. J. Jacobson, D. Broido, G. Chen, Z. Ren, and C.-W. Chu, Experimental study of the proposed super-thermal-conductor: BAs, Appl. Phys. Lett. **106**, 074105 (2015).

[14] See Supplemental Material at http://link.aps.org/supplemental/10.1103/PhysRevB.107.L081202 for computational details, expressions for the four-phonon, charge-impurity, and phonon-impurity scattering rates, plots of BAs spectral Q_{ph} and k_{ph} vs p, and S vs p including impurity scattering for BAs and Si, and phonon scattering rates, which includes Refs. [15–25].

[15] P. Giannozzi, S. Baroni, N. Bonini, M. Calandra, R. Car, C. Cavazzoni, D. Ceresoli, G. L. Chiarotti, M. Cococcioni, I. Dabo *et al.*, QUANTUM ESPRESSO: A modular and open-source software project for quantum simulations of materials, J. Phys. Condens. Matter **21**, 395502 (2009).

[16] P. Giannozzi, O. Andreussi, T. Brumme, O. Bunau, M. Buongiorno Nardelli, M. Calandra, R. Car, C. Cavazzoni, D. Ceresoli, M. Cococcioni *et al.*, Advanced capabilities for materials modelling with Quantum ESPRESSO, J. Phys. Condens. Matter **29**, 465901 (2017).

[17] Xi Chen, Chunhua Li, Fei Tian, Geethal Amila Gamage, Sean Sullivan, Jianshi Zhou, David Broido, Zhifeng Ren, and Li Shi, Thermal Expansion Coefficient and Lattice Anharmonicity of Cubic Boron Arsenide, Phys. Rev. Appl. **11**, 064070 (2019).

[18] Y. Okada and Y. Tokumaru, Precise determination of lattice parameter and thermal expansion of silicon between 300 and 1500 K, J. Appl. Phys. **56**, 314 (1984).

[19] S. Poncé, E. R. Margine, C. Verdi, and F. Giustino, EPW: Electron–phonon coupling, transport and superconducting properties using maximally localized Wannier functions, Comput. Phys. Commun. **209**, 116 (2016).

[20] F. Giustino, M. L. Cohen, and S. G. Louie, Electron-phonon interaction using Wannier functions, Phys. Rev. B **76**, 165108 (2007).

[21] C. Verdi and F. Giustino, Fröhlich Electron-Phonon Vertex from First Principles, Phys. Rev. Lett. **115**, 176401 (2015).

[22] K. Bushick, S. Chae, Z. Deng, J. T. Heron, and E. Kioupakis, Boron arsenide heterostructures: Lattice-matched heterointerfaces and strain effects on band alignments and mobility, npj Comput. Mater. **6**, 3 (2020).

[23] D. Chattopadhyay and H. J. Queisser, Electron scattering by ionized impurities in semiconductors, Rev. Mod. Phys. **53**, 745 (1981).

[24] S-i. Tamura, Isotope scattering of large-wave-vector phonons in GaAs and InSb: Deformation-dipole and overlap-shell models, Phys. Rev. B **30**, 849 (1984).

[25] T. Feng and X. Ruan, Quantum mechanical prediction of four-phonon scattering rates and reduced thermal conductivity of solids, Phys. Rev. B **93**, 045202 (2016).

[26] M. Fiorentini and N. Bonini, Thermoelectric coefficients of *n*-doped silicon from first principles via the solution of the Boltzmann transport equation, Phys. Rev. B **94**, 085204 (2016).

[27] The percentages in Fig. 2(b) refer to the ratios of the Q_{ph} values for Si and BAs at the corresponding densities. These ratios are different than the ratios of the corresponding Seebeck coefficients, which also include Q_c, the electronic Peltier thermopower through the Kelvin-Onsager relation: $S = Q_c + Q_{ph}$.

[28] P. G. Klemens, Theory of phonon drag thermopower, in *Proceedings of the Fifteenth International Conference on Thermoelectrics*, edited by T. Caillat (IEEE, New York, 1996), pp. 206–208.

[29] L. Lindsay, D. A. Broido, and T. L. Reinecke, First-Principles Determination of Ultrahigh Thermal Conductivity of Boron Arsenide: A Competitor for Diamond? Phys. Rev. Lett. **111**, 025901 (2013).

[30] T. L. Feng, L. Lindsay, and X. L. Ruan, Four-phonon scattering significantly reduces intrinsic thermal conductivity of solids, Phys. Rev. B **96**, 161201(R) (2017).

[31] J. S. Kang, M. Li, H. A. Wu, H. Nguyen, and Y. J. Hu, Experimental observation of high thermal conductivity in boron arsenide, Science **361**, 575 (2018).

[32] S. Li, Q. Zheng, Y. Lv, X. Liu, X. Wang, P. Y. Huang, D. G. Cahill, and B. Lv, High thermal conductivity in cubic boron arsenide crystals, Science **361**, 579 (2018).

[33] F. Tian, B. Song, X. Chen, N. K. Ravichandran, Y. Lv, K. Chen, S. Sullivan, J. Kim, Y. Zhou *et al.*, Unusual high thermal conductivity in boron arsenide bulk crystals, Science **361**, 582 (2018).

[34] B. Liao, B. Qiu, Ji. Zhou, S. Huberman, K. Esfarjani, and G. Chen, Significant Reduction of Lattice Thermal Conductivity by the Electron-Phonon Interaction in Silicon with High Carrier Concentrations: A First-Principles Study, Phys. Rev. Lett. **114**, 115901 (2015).

[35] T.-H. Liu, B. Song, L. Meroueh, Z. Ding, Q. Song, J. Zhou, M. Li, and G. Chen, Simultaneously high electron and hole mobilities in cubic boron-V compounds: BP, BAs, and BSb, Phys. Rev. B **98**, 081203(R) (2018).

[36] N. K. Ravichandran and D. Broido, Unified first-principles theory of thermal properties of insulators, Phys. Rev. B **98**, 085205 (2018).

[37] M. Strasser, R. Aigner, C. Lauterbach, T. F. Sturm, M. Franosch, and G. Wachutka, Micromachined CMOS thermoelectric generators as on-chip power supply, Sens. Actuators A **114**, 362 (2004).

[38] F. Mancarella, A. Roncaglia, and G. C. Cardinali, A measurement technique for thermoelectric power of CMOS layers at the wafer level, Sens. Actuators A **132**, 289 (2006).

[39] A. Stranz, J. Kähler, A. Waag, and E. Peiner, Thermoelectric properties of high-doped silicon from room temperature to 900 K, J. Electron. Mater. **42**, 2381 (2013).

[40] J. Kim, D. A. Evans, D. P. Sellan, O. M. Williams, E. Ou, A. H. Cowley, and L. Shi, Thermal and thermoelectric transport measurements of an individual boron arsenide microstructure, Appl. Phys. Lett. **108**, 201905 (2016).

[41] J. Xing, X. Chen, Y. Zhou, J. C. Culbertson, J. A. Freitas, E. R. Glaser, J. Zhou, L. Shi, and N. Ni, Multimillimeter-sized cubic boron arsenide grown by chemical vapor transport via a tellurium tetraiodide transport agent, Appl. Phys. Lett. **112**, 261901 (2018).

[42] X. Chen, C. Li, Y. Xu, A. Dolocan, G. Seward, A. Van Roekeghem, F. Tian, J. Xing, S. Guo, N. Ni *et al.*, Effects of impurities on the thermal and electrical transport properties of cubic boron arsenide, Chem. Mater. **33**, 6974 (2021).

[43] D. K. C. MacDonald, *Thermoelectricity: An Introduction to the Principles* (Wiley, New York, 1962).

[44] A. Jain and A. J. H. McGaughey, Thermal transport by phonons and electrons in aluminum, silver, and gold from first principles, Phys. Rev. B **93**, 081206(R) (2016).

[45] Z. Tong, S. Li, X. Ruan, and H. Bao, Comprehensive first-principles analysis of phonon thermal conductivity and electron-phonon coupling in different metals, Phys. Rev. B **100**, 144306 (2019).

[46] J. Shin, G. Amila Gamage, Z.i Ding, K. Chen, F. Tian, X. Qian, J. Zhou1, H. Lee, J. Zhou, L. Shi *et al.*, High ambipolar mobility in cubic boron arsenide, Science **377**, 437 (2022).

[47] S. Yue, F. Tian, X. Sui, M. Mohebinia, X. Wu, T. Tong, Z. Wang, B. Wu, Q. Zhang, Z. Ren, J. Bao, and X. Liu, High ambipolar mobility in cubic boron arsenide revealed by transient reflectivity microscopy, Science **377**, 433 (2022).

[48] M. Markov, S. E. Rezaei, S. N. Sadeghi, K. Esfarjani, and M. Zebarjadi, Thermoelectric properties of semimetals, Phys. Rev. Mater. **3**, 095401 (2019).